Volume 17, Issue 1, 172504 (1-13)

Iranian Journal of Earth Science (IJES)

https://dx.doi.org/10.57647/j.ijes.2025.1701.04

Geochemistry and technomagmatic environment of Eocene volcanic rocks in Yuzbashi Chay region, west of Qazvin (Iran)

Saman Salehpour[1], Mohammad Ali Arian[2,*], Alireza Jafari Rad[1], Reza Zarei Sahamieh[3], Abdollah Yazdi[4]

[1]*Department of Geology, Science and Research Branch, Islamic Azad University, Tehran, Iran.*
[2]*Department of Geology, North Tehran Branch, Islamic Azad University, Tehran, Iran.*
[3]*Department of Geology, Lorestan University, Khorramabad, Iran.*
[4]*Department of Geology, Kahnooj Branch, Islamic Azad University, Kahnooj, Iran.*

[*]**Corresponding author:** maa1361@yahoo.com

Original

Received:
17 February 2024
Revised:
9 May 2024
Accepted:
8 August 2024
Published online:
10 January 2025

Abstract:

The study area is 92 km northeast of Zanjan City (Iran), north of the Tehran-Tabriz freeway. The rock units outcropped in the Zanjan quadrangle include the Precambrian and the Quaternary from the old to the new. However, the volcanic rocks in this vast area are of Eocene age and younger. Volcanic rocks include acidic, rhyolitic, rhyodacite, andesitic lavas, along with tuff and ignimbrite. From the mineralogical perspective, these volcanic rocks have low contents of quartz, low alkaline feldspar, and abundant plagioclase and pyroxene. In addition, porphyritic, microlithic porphyry, glomeroporphyritic, and poikilitic textures are dominant in these rocks. Geochemical studies based on oxides of major and Minor elements indicate the calc-alkaline nature of these volcanic rocks. Furthermore, studying the change trends in major, trace, and rare earth elements demonstrates a connection and affiliation between different rock groups. These rocks have formed during the subduction process and probably originate from a lower crustal source.

Keywords: Volcanic rocks; Subduction environment; West Qazvin; Iran

1. Introduction

The study area covers the northeast part of the 1:100,000 Abhar map, 92 km southeast of Zanjan city and north of the Tehran-Tabriz freeway. This area has geographical coordinates of 49° 26′ to 49° 30′ E 36° 22′ to 36° 30′ E with an area of 55 km^2. Geologically, it belongs to the Zanjan quadrangle. Also, in terms of geological and structural divisions of Iran, it is a part of Western Alborz, according to (Stocklin, 1968) and (Nabavi, 1976), respectively (Fig. 1a). The Cenozoic magmatic activity of Alborz, which is mostly of Paleogene age, is equivalent to Karaj Formation in stratigraphic divisions (Stocklin, 1968; Annells et al., 1975). Some researchers believe that Karaj Formation rocks have formed in a continental setting and depend on subduction in the north direction and along the Zagros (Asiabanha et al., 1989; Zanchi et al., 2006; Arjmandzadeh et al., 2020; Mollai et al., 2021). Some have considered the age of equivalent units in western Qazvin equivalent to the Oligocene (Asiabanha, 2001). Following the seafloor volcanic activity in Alborz, large volumes of intermediate to basaltic lavas have erupted through surface fissures (Mobashergarmi, 2013). The origin of these volcanic lavas is a subduction-dependent zone with a small share of asthenospheric melt (Shafaii Moghadam and Shahbazi Shiran, 2010).

2. Geology of the study area

From the lithostratigraphic perspective, the rock units of the region can be divided into two parts: A) volcanic and pyroclastic rocks (Karaj Formation), and B) plutonic and subvolcanic massifs. Volcanic rocks are mostly rhyodacitic, dacitic, and intermediate acidic such as trachyandesite, andesite, and basaltic andesite. These rocks are observed

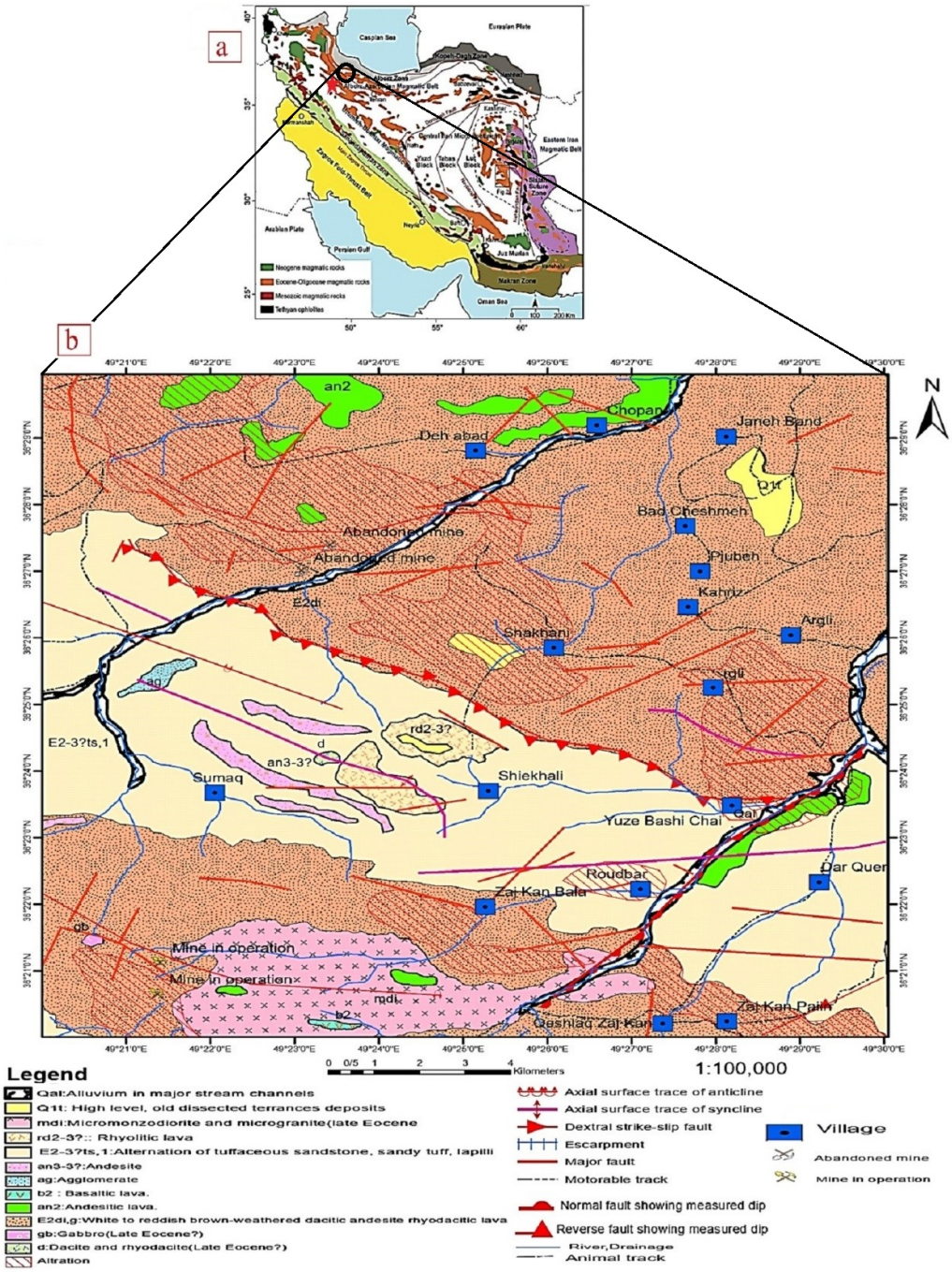

Figure 1. a) The study area in the geological map of Iran (Moghadam et al., n.d.) and b) the location of the Yuzbashi Chay region in the 1:100000 map of Qazvin (from (Sarikhani et al., 2017)).

along with sandy tuffs, lapilli tuffs, and breccia. Paleogene volcanic rocks are very thick and are mainly formed during three volcanic phases. With the Eocene age, the first phase consists of submarine tuffs with (Karaj Formation) sediments. The rocks of this phase are divided into two members: Kurdkand and Amand. Kordkand member starts with alternating sandstone and tuff mudstone and ends with mudstone. Amand member also starts with a tuff sandstone and ends with tuff mudstone and sandstone with alternating lava and tuff. In the north of the Yuzbashi region, the second phase of volcanic activity during the Eocene consists of basic eruptions in the terrestrial environment and mostly of the trachybasalt type (Fig. 1b). In the third phase, which occurred in the Oligocene, volcanic eruption activities have been intense. Due to these activities, large volumes of rhyolite and dacite were exposed along with associated tuffs and ignimbrite. As a result, the Tarom region is entirely covered by a large thickness of these lavas (Aghazadeh et al., 2011; Ghasempour et al., 2014; Teshnizi et al., 2022; Nazari et al., 2023; Ousta et al., 2024). According to (Dilek et al., 2010), the second and third phases occurred during the Oligocene and represent the extension environment and intensity of the movements of the Alborz plate. The main expansion of this phase is in the western part of the region. Jahangiri (2007) suggested the Oligo-Miocene age for these rocks. In terms of corrosion faults, there are generally three

categories of faults with north-south, northeast-southwest, and northwest-southeast trends in the study area. The joints in the study area can be attributed to tectonic movements following the compressive phase in the study area. Copper, lead, and zinc mineralizations have occurred mainly along the joints and fractures of pyroclastic rocks. In the rose diagram prepared by (Zarei Sahamieh, 1992), three distinct fracturing directions can be identified: 1) Extension joints (longitudinal) whose direction is parallel to the fold axis, 2) Diagonal or conjugate joints that intersect these planes perpendicular to the fold axis, and 3) Extension joints perpendicular to the fold axis. The above joints and fractures are caused by cooling the intrusive mass, folds due to the Pyrenean orogenic phase, and folds due to the impact of the last phase of the Alpine orogeny. Mineralization has taken place along the above fractures and joints. However, the highest mineralization concentration is along the joints parallel to the extension joints.

3. Study method

During field surveys, 100 samples were taken systematically, of which 50 thin sections were prepared to determine the amount of main, secondary, and rare elements in rock samples. For this purpose, 19 samples from rock mass were selected and sent to Zarazma Mineral Studies Company for inductively coupled plasma by mass spectrometry (ICP-MS). Also, 6 thin-polished sections were selected to perform thermobarometry studies on the andesitic basalts and andesites in the study area. In addition, 15 amphibole, pyroxene, and plagioclase minerals were microproped through point analyses. Point analysis was performed on minerals using an Electron Probe Micro Analyzer XPMA in Binalood ore (HORIBA, XGT-7200). The device was equipped with a 50 kV accelerator voltage and current intensity of 1. The tests were performed in points with a diameter of 10 μm for 80 seconds for each point. Structural formulas were calculated using Excel spreadsheets made for minerals.

4. Lithography

In this step, we conducted the petrological study of various volcanic rocks from the study area, including basalt, basaltic andesite, andesite, trachyandesite, trachyte, rhyolitic tuff, and rhyodacite.

A) Rhyolitic to Rhyodacitic tuff: In hand samples, they appear dark gray and contain fine crystals, sometimes without any crystals. Under the microscope, they show plagioclase and alkali feldspar crystals of sanidine type with Carlsbad twins along with pyroxene and biotite. Histologically, they have porphyry, hialoporphyritic, microlithic porphyry, and glomeroporphyritic. Iron oxides or opaque minerals are the accessory minerals of these rocks and makeup about 5 vol.% of the rock. Secondary minerals of these rocks include calcite, chlorite, epidote, and iron oxides produced through the decomposition of plagioclases. Iron oxides also appear in the matrix of these rocks (Fig. 2a).

B) Basaltic andesite: This sample is seen in a macroscopic scale or hand sample in a dark gray color. Under the microscope, they show plagioclase and pyroxene phenocrysts in a fine-grained matrix. These rocks have porphyritic, microlithic porphyritic, hialoporphyritic, and glomeroporphyritic textures. Plagioclases are anhedral to subhedral and

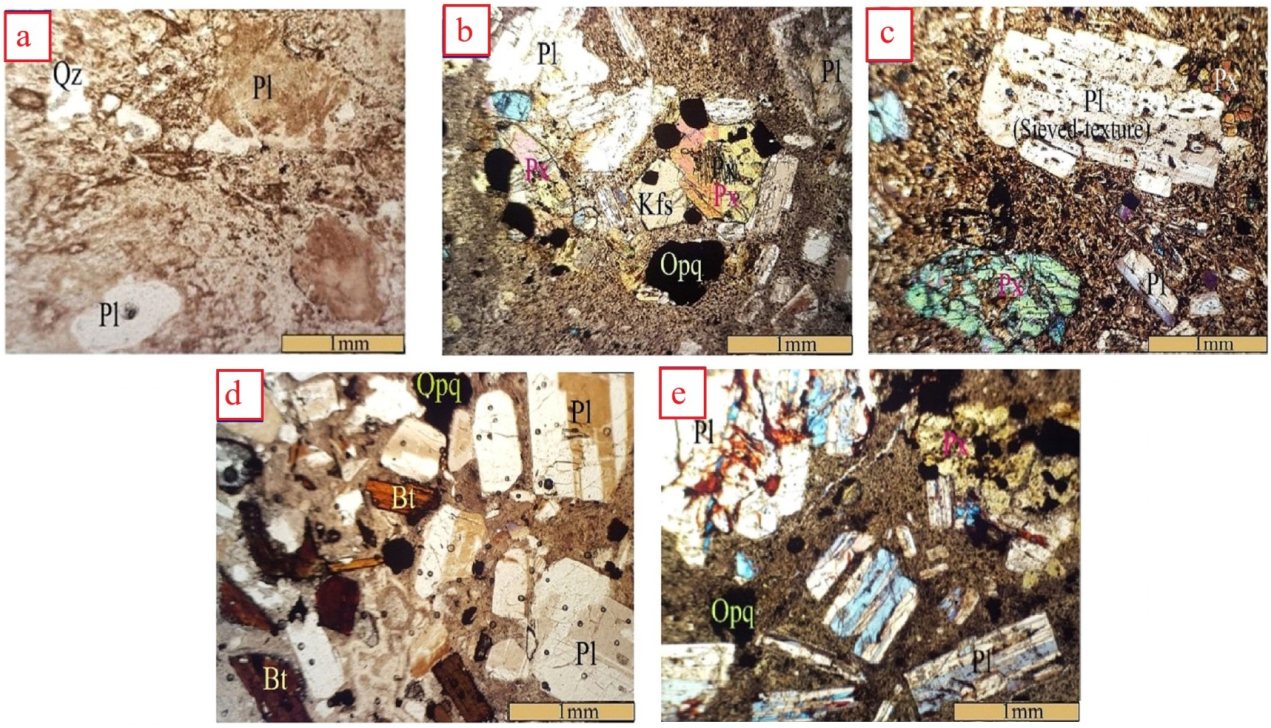

Figure 2. a) The presence of plagioclase and quartz as the main minerals in rhyolite to rhyodacite tuff, b) plagioclase minerals (with banded and zoned twins), pyroxene, alkaline feldspar, and opaque minerals in basalt, c) plagioclase minerals (with sieve texture, polysynthetic) and pyroxene in basaltic andesite, d) Euhedral to subhedral crystals of plagioclase and biotite in trachyandesite, and e) Microscopic section of pyroxene, opaque minerals, and twin-bearing plagioclases in basaltic andesite (all minerals were investigated under the XPL light).

have a polysynthetic twinning or zoning structure. Most of these crystals are saussuritized along with the twins and centers. Based on extinction angle measurements (An 34 – 38), the rocks are of oligoclase-andesin type. Along the twins and on the decomposed surface, its effects can be seen on the crystal surfaces. Some pyroxenes have been decomposed into filamentous amphiboles or auralites. The accessory mineral of these rocks is olivine, which has been metamorphosed into serpentine. Calcite, chlorite, epidote, and serpentine Iron oxides are the secondary minerals of this rock, generated due to the decomposition of plagioclase and mafic minerals. Opaque minerals and iron oxides are also observed in the rock matrix (Fig. 2c).

C) Andesites: They are seen in macroscopic scale or hand sample as gray to grayish pink. Under the microscope, they show plagioclase and pyroxene phenocrysts placed in a microcrystalline matrix. They have porphyritic, microlithic porphyritic, hialoporphyritic, and glomeroporphyritic textures. Plagioclases are euhedral to subhedral and have polysynthetic twinning and, sometimes, a zoning structure. Based on the extinction angle measurement (An 28 – 34), they are oligoclase-andesine type. Pyroxene crystals show the properties of augite and possibly Aegirine augite. The opaque minerals are the accessory minerals of these rocks, making up about 5% of the rock in thin-section samples. Calcite, sericite, chlorite, and iron oxides, as the secondary minerals of these rocks, have resulted from the decomposition of plagioclase and pyroxene (Fig. 2c and 2e).

D) Basalt: Basalt is seen as gray to dark gray in the field and hand sample. Under a microscope, plagioclase phenocrysts are highly altered, and pyroxene crystals are anhedral. They have porphyritic and glomeroporphyritic textures. Some plagioclase minerals show a zoning structure and have completely degraded to chlorite and calcite. Based on their extinction angle measurement (An 28 – 36), they are of the oligoclase-andesine type. In terms of their frequency, they make up 25 to 30 vol.% of the rock sections. Based on crystallographic and optical properties, pyroxenes are of the augite type. These minerals, together with plagioclase, show an ophitic texture. In terms of their frequency, they make up 10 to 15 vol.% of the rock in the thin section. Accessory minerals are often iron oxides or opaques. Also, the secondary minerals of these rocks are calcite, chlorite, epidote, clay minerals, and iron oxides such as hematite, which are produced through the degradation of plagioclase and pyroxene (Fig. 2b).

E) Trachyandesites: These rocks appear gray to dark gray in the field. Under the microscope, they contain plagioclastic and biotite microcrystals. The texture of these rocks is porphyritic and glomeroporphyritic. Plagioclase is seen as euhedral to subhedral fine crystals that cannot be identified due to decomposition. In terms of their frequency, they make up 10 to 1 vol.% of rock. Biotite crystals with parallel faces are well detected in the thin-section samples. They have a direct extinction angle and appear brown to dark brown. About 5 to 10 vol.% of the rock matrix is included. The secondary minerals of these rocks are iron oxides found in the rock matrix. The secondary minerals of these rocks are calcite, chlorite, sericite, and iron oxides such as goethite which have formed because of plagioclase decomposition. In some samples, zircon inclusions are observed inside the biotite. Quartz minerals appear as microcrystals in a very small amount (< 5 vol.%). Fine and needle-shaped apatite crystals are observed inside the quartz minerals (Fig. 2d).

5. Geochemistry of studied rocks

Chemical effects of different processes, including differential crystallization, magmatic mixing, contamination, or a mixture of these processes, can be distinguished through geochemical studies. The distribution and dispersion of various elements in the rock units of each region and the relationship and dependence of these elements are among the most important aspects usually considered in geochemical studies (Tables 1 and 2). Using these relationships provides an insight into the environment and processes affecting the rock genesis to some extent. The rock samples in the Yuzbashi Chay region contain high contents of SiO_2 (58.17 to 67.51 wt.%) and K_2O + Na_2O (10.09 to 5.98 wt.%) (Tables 3 and 4). Based on the K_2O + Na_2O versus SiO_2 diagram (Midlmust et al., 1994), they lie in the range of basaltic andesite, andesite-trachyandesite, and dacite-trachydacite. Most of the samples in this diagram are in the sub-alkaline field (Fig. 3a). The SiO_2 vs. Zr/TiO_2 diagram proposed by Floyd and Winchester (1977) was used for more accurate identification of the studied rocks. In this diagram, the studied specimens lie in the range of andesite, trachyandesite, and dacite-rhyodacite (Fig. 3b). The K_2O vs. SiO_2 (LeBass et al., 1986) diagram was used to segregate calc-alkaline, high-potassium calc-alkaline and shoshonite rocks of the study area (Fig. 3c). As shown in Fig. 3c, these rocks are in the range of high-potassium calc-alkaline to shoshonite. According to the alkali-alkaline modified index chart presented by (Frost et al., 2001), rock samples of the study area are in the range of alkali calcic to alkali (Fig. 3d). The formation of shoshonite magmas has been attributed to the partial melting of the metasomatic lithosphere Conceicao and Green (2004). The segregation of aqueous fluids from sediments subducted deep in the mantle, and the reaction between these fluids with the mantle has led to the formation of potassic magmas. This point is also confirmed by experimental data (Wyllie and Skine, 1982; Jiang et al., 2002).

Based on the primitive mantle-normalized spider diagram Sun and McDonough (1989) shown in Fig. 4, volcanic rocks of Yuzbashi Chay show enrichment in LILEs and LREEs (Cs, Pb, and K) compared to HFSEs (Ti, P, and Nb). This feature is similar to that of igneous rocks formed in subduction zones (Perfit et al., 1980; Pearce and Peate, 1995). This diagram shows obvious positive anomalies in U, K, and Pb and a sharp negative anomaly in P, Zr, and Ti. This observation suggests that apatite, zircon, titanium magnetite and magnetite are more differentiated in these rocks and have a negative anomaly than Ba and Sr. In addition, Ti and Nb anomalies can also be suggestive of crustal contamination or remelting (Swain et al., 2008). In subduction zones, trace elements and the radiogenic isotope composition of magma are mainly controlled by the fluids that transport elements from the subduction crust to the mantle wedge.

Table 1. Chemical composition of rocks (major oxides in % and trace elements in ppm).

Samples	S-54	S-56	S-64	S-70	S-75	S-81	S-87	S-90	S-103	S-106
Rock	Andesite		TrAn	B TrAn	Dacite-Trachy dacite			BasalticTrachy andesite		Andesite
SiO_2	56.11	57.12	57.04	52.95	66.08	61.33	67.08	51.17	53.57	58.49
TiO_2	0.84	0.77	0.84	0.97	0.47	0.65	0.46	0.97	0.78	0.76
Al_2O_3	16.66	16.7	16.73	17.71	15.95	15.9	15.68	17.73	20.32	19.42
TFe_2O_3	7.42	6.89	6.95	8.04	2.69	5.36	2.57	8.15	7.37	6.5
MnO	3.09	3.32	3.07	3.65	0.72	2.19	0.83	2.96	2.95	2.23
MgO	0.13	0.19	0.18	0.16	0.14	0.1	0.09	0.15	0.15	0.1
CaO	5.13	5.72	4.83	7.76	2	3.66	1.03	6.94	5.01	5.09
Na_2O	3.5	3.22	3.35	3.66	4.82	3.57	4.73	3.53	3.7	3.42
K_2O	3.32	2.85	4.21	2.32	5.27	4.98	6.02	3	3.25	2.79
P_2O_5	0.23	0.23	0.25	0.27	0.12	0.21	0.1	0.28	0.3	0.24
BaO	0.05	0.05	0.07	<	0.07	0.05	0.08	0.05	0.05	0.05
SO_3	0.07	0.07	0.06	0.11	0.05	0.08	<	<	<	<
LOI	3.46	2.88	2.42	2.34	1.62	1.93	1.34	5.08	2.55	0.9
Total	100.01	100.01	100	99.94	100	100.01	100.01	100.01	100	99.99
Na_2O/K_2O	1.05	1.13	0.8	1.58	0.91	0.72	0.79	1.18	1.14	1.23
Na_2O+K_2O	6.82	6.07	7.56	5.98	10.09	8.55	10.75	6.53	6.95	6.21
A/CNK	0.89	0.89	0.89	0.78	0.92	0.89	0.97	0.82	1.08	1.08
A/NK	1.78	1.99	1.66	2.07	1.17	1.41	1.1	1.96	2.11	2.24
Li	19	23	35	27	23	19	37	32	28	25
Be	1.9	2	1.8	1.8	4.1	2.7	3.8	2	2	2.1
Sc	19.1	16.9	17.2	23.7	4.4	11.5	4.2	20.8	17.4	14.8
V	194	183	186	252	32	161	43	252	225	174
Cr	53	37	27	47	21	35	19	49	37	37
Co	21.7	20.4	19.8	24.8	<1	13.5	<1	24.4	21.5	17.2
Ni	14	16	12	13	6	15	4	12	12	11
Cu	74	62	41	68	9	61	10	83	46	49
Zn	67	66	82	71	54	48	58	72	71	64
As	10.9	11.3	13.9	23.4	16.4	19.5	52.8	11.6	22.5	25
Rb	71	65	72	52	145	146	172	78	97	93
Sr	423	483	462	621	343	519	231	519	668	505
Y	26.2	22.3	23.4	23.7	26.6	23.9	26.4	23.3	22.3	23.7
Zr	168	164	183	175	372	156	416	171	156	213
Nb	12.4	8.7	7.6	10.4	15.1	15.7	18.3	12.6	9.2	13.6
Cs	0.7	1.7	2.8	0.9	2	2.5	2.2	2.3	5.9	10.1
Ba	657	637	876	530	1000	724	990	593	743	644
La	26	26	24	25	53	33	53	25	28	26
Ce	56	56	56	53	117	68	119	54	57	61
Pr	5.97	6.03	5.8	5.58	10.7	7	10.9	5.74	6.07	6.28
Nd	22.7	23.1	22.1	22.4	38	25.4	37.9	22.2	23.2	24
Sm	4.5	4.29	4.65	4.19	6.64	4.89	6.54	4.38	4.72	4.58
Eu	1.59	1.55	1.75	1.59	2	1.57	1.97	1.67	1.71	1.57
Gd	3.62	3.56	3.55	3.51	4.76	3.79	4.72	3.53	3.55	3.7
Tb	0.65	0.62	0.64	0.63	0.75	0.64	0.76	0.63	0.61	0.65
Dy	4.03	3.85	3.84	3.8	4.4	3.91	4.58	3.76	3.73	4.23
Er	2.22	2.06	2.11	2.08	2.63	2.15	2.6	1.99	1.95	2.27
Tm	0.32	0.33	0.33	0.31	0.41	0.34	0.42	0.3	0.28	0.35
Yb	3	2.7	2.8	3.2	1.8	2.4	1.6	3.2	3	2.7
Lu	0.38	0.37	0.37	0.34	0.49	0.42	0.5	0.35	0.34	0.42
Ta	0.93	0.62	0.55	1.2	1.01	1.13	0.89	0.89	1.11	1.04
W	1.3	1	1	1.4	1.9	2.1	2.2	2.9	2.2	1.6
Pb	1	1	1	1	18	5	8	1	1	1
Th	7.94	9	7.03	8.44	22.44	21.24	24.31	10.6	6.95	10.28
U	2.4	2.52	2.1	2.8	6.7	5.7	6.5	2.7	2.15	3.5
Hf	4.12	3.98	4.16	4.06	8.37	4.03	9.46	4.09	3.42	5.11
Mg#	50	54	52	52	39	50	44	47	49	45
Eu/Eu*	1.21	1.22	1.32	1.27	1.09	1.12	1.09	1.31	1.28	1.17

Table 2. Chemical composition of rocks (major oxidesin % and trace elements in ppm).

Samples	S-110	S-114	S-117	S-120	S-123	S-128	S-134	S-139	S-147
Rock	Andesite			Dacite-trachy dacite					TrAn
SiO_2	57.64	58.08	58.13	62.47	63.19	63.91	63.56	63.95	58.78
TiO_2	0.73	0.73	0.76	0.45	0.42	0.38	0.4	0.39	0.68
Al_2O_3	19.64	19.49	19.43	18.82	18.75	18.12	18.7	18.05	16.89
TFe_2O_3	6.47	6.24	6.05	4.1	3.89	3.67	3.61	3.64	6.38
MnO	2.51	2.4	2.26	0.9	1.37	0.8	0.62	1.04	2.58
MgO	0.09	0.09	0.08	0.08	0.06	0.1	0.07	0.05	0.1
CaO	5.18	5.03	4.98	3.76	3.14	3.13	3.05	3.19	4.53
Na_2O	3.28	3.24	3.39	3.51	3.91	3.45	3.35	3.71	2.74
K_2O	2.58	2.54	2.63	3.64	3.55	3.68	4.04	4.47	3.37
P_2O_5	0.22	0.25	0.25	0.17	0.18	0.16	0.15	0.16	0.19
BaO	<	<	0.05	0.06	0.07	0.07	0.07	0.07	0.05
SO_3	<	<	<	<	<	<	<	<	
LOI	1.67	1.91	2	2.03	1.48	2.52	2.38	1.27	3.71
Total	100.01	100	100	99.99	100.01	99.99	100	99.99	100
Na_2O/K_2O	1.27	1.28	1.29	0.96	1.1	0.94	0.83	0.83	0.81
Na_2O+K_2O	5.86	5.78	6.02	7.15	7.46	7.13	7.39	8.18	6.11
A/CNK	1.11	1.13	1.11	1.14	1.17	1.18	1.21	1.08	1.03
A/NK	2.4	2.41	2.3	1.94	1.82	1.87	1.89	1.65	2.07
Li	46	38	32	26	27	25	23	30	40
Be	1.5	1.6	1.6	2	2	2.3	2.3	2.1	1.6
Sc	11.6	12.6	12.3	6.1	5.5	5.1	5.3	5.5	13.9
V	141	143	142	74	71	54	69	71	136
Cr	34	29	31	21	20	22	20	24	70
Co	13.8	14	14	6.3	5.8	4	4.4	5.2	17.9
Ni	6	5	6	7	5	4	5	6	21
Cu	47	38	58	23	22	25	19	18	42
Zn	42	52	57	40	35	33	29	31	39
As	16.8	21.1	18.2	10.5	8.7	12.9	11.2	15.7	17
Rb	94	88	81	110	77	92	105	120	93
Sr	398	404	403	441	438	384	378	401	348
Y	19	18.9	19.6	13.5	12.7	12.8	12.8	13.7	14.8
Zr	160	175	183	54	49	47	47	56	111
Nb	12.6	13.3	13.1	9.5	9.5	9.9	11	11.8	8.8
Cs	13	15.4	10.4	3.2	2.1	3.4	3.6	1.5	4.3
Ba	526	536	549	672	662	675	695	720	554
La	20	20	22	24	24	24	25	25	16
Ce	46	48	50	44	44	44	44	45	33
Pr	6.18	6.31	6.4	5.76	5.7	5.78	5.61	5.86	4.36
Nd	23.1	24	25	19.7	20	20.2	19.3	20.9	17
Sm	4.38	4.65	4.97	3.64	3.56	3.73	3.5	3.64	3.29
Eu	1.55	1.56	1.68	1.5	1.48	1.5	1.51	1.5	1.31
Gd	3.63	3.61	3.82	2.96	3.07	3.04	2.86	3.09	2.81
Tb	0.64	0.64	0.68	0.47	0.5	0.48	0.45	0.48	0.51
Dy	3.9	3.94	4.31	2.51	2.63	2.64	2.35	2.57	3.04
Er	2.19	2.13	2.42	1.35	1.41	1.39	1.26	1.33	1.68
Tm	0.35	0.32	0.37	0.2	0.21	0.21	0.2	0.21	0.25
Yb	2.2	2.2	2.2	1.4	1.3	1.3	1.3	1.3	2.1
Lu	0.39	0.37	0.42	0.26	0.26	0.26	0.25	0.28	0.31
Ta	1.02	1.07	0.99	0.75	0.84	1.17	0.96	1.19	0.67
W	1.6	1.6	1.5	1.3	1.2	1.6	1.7	1.6	1.1
Pb	1	1	1	3	1	2	5	2	1
Th	9.53	9.04	8.98	8.01	8.45	8.59	9.11	9.45	7.72
U	2.8	2.7	2.7	1.8	2	2.18	2	2.6	2.1
Hf	4.65	4.89	5.44	1.62	1.8	1.64	1.53	1.92	3.22
Eu/Eu*	1.19	1.17	1.19	1.4	1.38	1.37	1.47	1.37	1.32
Mg#	48	48	47	34	46	34	29	41	49

Table 3. determining the type of plagioclase using Spreadsheet.

Rock name	Sample	An	Ab	Or
Basalt	S 114	74.216	24.52	1.260
Basaltic andesite	S 106	89.949	8.56	1.483
Andesite	S 139	47.803	45.96	6.23
Andesite basalt to basalt	S 117	59.578	35.24	5.17
Andesite basalt to basalt	S 117	70.234	24.80	4.95
Basaltic anddesite to basalt	S 54	99.95	0	0.048
Basaltic andesite	S 106	95.93	3.69	0.36

Table 4. Determining the type of plagioclase and pyroxene using an Excel spreadsheet.

Sample No.	Wo	En	Fs
S117	59.00563	35.20067	5.793703
S106	95.60706	0	4.392935
S106	95.64433	0	4.355665
S106	95.69973	0	4.300272
S114	96.90859	0	3.09141
S64	60.06532	39.93468	0
S54	93.96988	0	6.030117

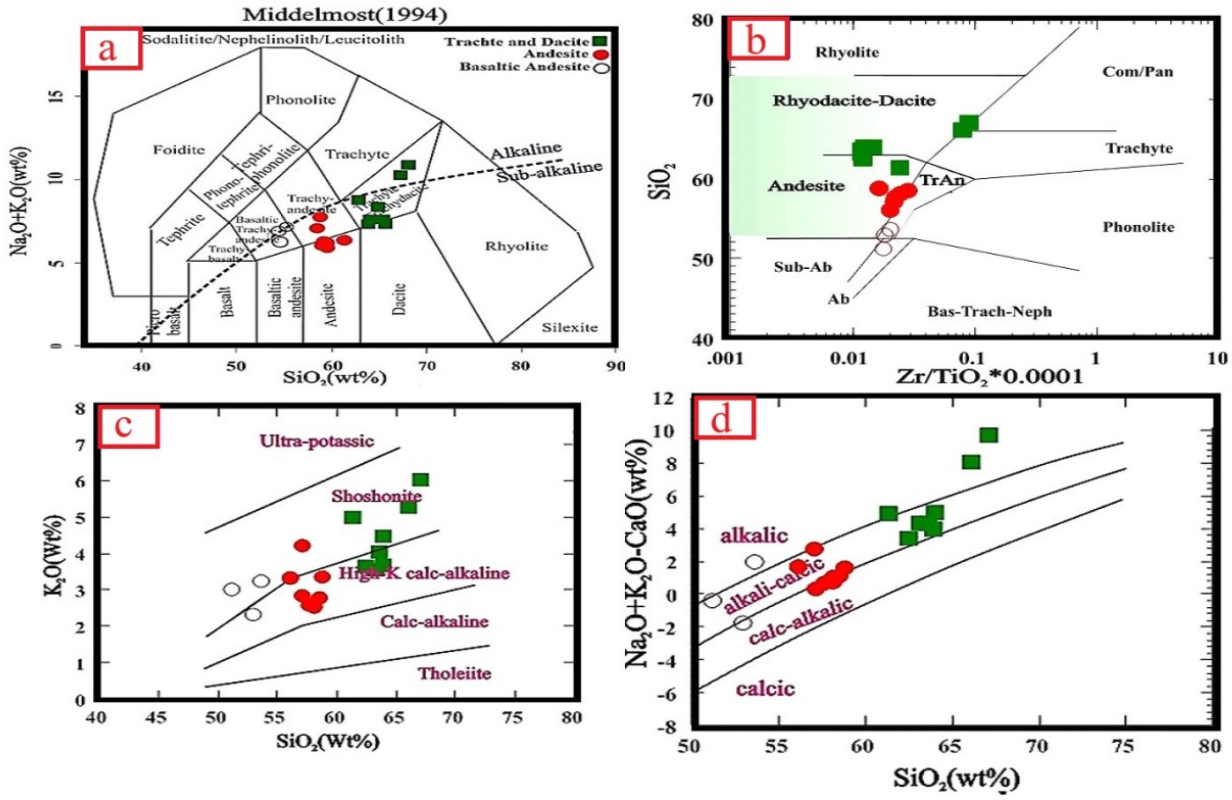

Figure 3. a) diagram classification (Midlmust et al., 1994) for Yuzbashi Chay volcanic rocks; samples are in the range of basaltic andesite, andesite, and dacite-trachydacite, b) the studied samples are in the range of andesite, trachyandesite, and dacite-rhyodacite, c) K_2O vs. SiO_2 (LeBass et al., 1986) diagram; the volcanic rocks of the study area are in the range of high k calc-alkaline to shoshonite, and d) $Na_2O + K_2O$-CaO vs. SiO_2 (Frost et al., 2001); samples lie in the range of calcic to alkali.

Therefore, the mantle is expected to be enriched in LILEs (e.g., Cs, Rb, and U) and LREEs (water-soluble elements such as Th and Pb). On the other hand, it will be depleted from HSFEs (e.g., Nb, Ta, Ti, Zr, and Hf) and HREEs, but enriched in Pb, leading to negative Nb-Ta anomalies and positive Pb anomalies (Zheng, 2019). (Kamber et al., 2002) believe there is a positive Pb anomaly due to metasomatism of mantle wedge caused by fluids from the subducted crust or magma contamination with continental crust. In general, significant negative anomalies of HFSEs (e.g., Nb, Ti, and

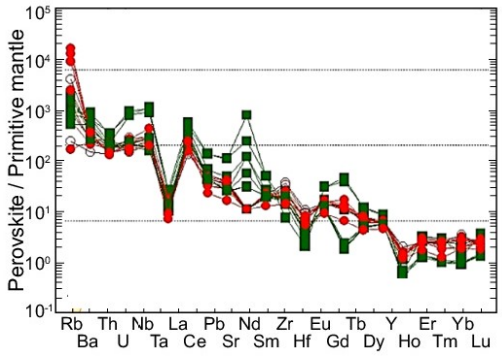

Figure 4. Trace elements variation in the primitive mantle-normalized diagram (Sun and McDonough, 1989).

Zr) and positive anomalies of LILEs (e.g., Cs, K, Th and U) are inferred from the properties of magmas related to subduction zones (Gill, 2010; Leuthold et al., 2013) and the generated magmas are related to an arc environment (Kelemen et al., 2003). LILE enrichment is caused by adding water-soluble elements by fluids derived from melting a dehydrated subducted piece crust into a mantle wedge (Tatsumi et al., 1986). However, due to the immobility of the HFSE elements in these fluids, HFSE depletion suggests the previous depletion of these elements in the mantle wedge (Elliott, 2003). Hence, the fluids released have higher LILE and LREE concentrations than HFSEs.

In this study, Keskin (2002) diagrams were used to determine factors controlling the distribution of trace and rare elements abundance during fractional crystallization in volcanic rocks. Geochemical modeling of Yuzbashi Chay volcanic rocks shows that different minerals have been involved in amount changes of incompatible elements. These minerals control the amount of the elements during differential crystallization. Based on the modeling results and the trend of LREEs and HREEs, partial melting is mainly controlled by garnet (Figs. 5a and 5b). Fig. 5c represents the HFSEs (e.g., Nb, P, and Ti) adsorbed by clinopyroxene, ilmenite, and apatite from the melt. Studying LILEs (Ba, Sr, and Rb) shows that plagioclase and biotite were the main factors controlling and distributing these elements (Figs. 5e and 5f). In other words, negative anomalies of Nb, P, Ti, and Ba can be due to differentiation of ilmenite, plagioclase, biotite, and, probably, apatite. The differentiation of these minerals is also consistent with their petrographic properties.

The tectonic environment of Yuzbashi Chay volcanic rocks was evaluated using graphs designed based on the abundance of trace elements inactivity vs. alteration and weathering processes (Pearce et al., 1984). These diagrams are used to segregate continental and arc-related tectonic environments. Based on the (Rb/30-Hf-Ta × 3) diagram (Harris et al., 1986) in Fig. 6a, most of the samples are in the volcanic arc and post-collisional range. Also, Rb vs. Y + Nb diagram ((Pearce et al., 1984)Fig. 6b) suggests a VAG range for the studied samples, and most of these samples are in the Post-COLG range. In addition, according to the Th/Yb vs. La/Yb and Nb/Yb vs. Th/Yb diagrams ((Pearce et al.,

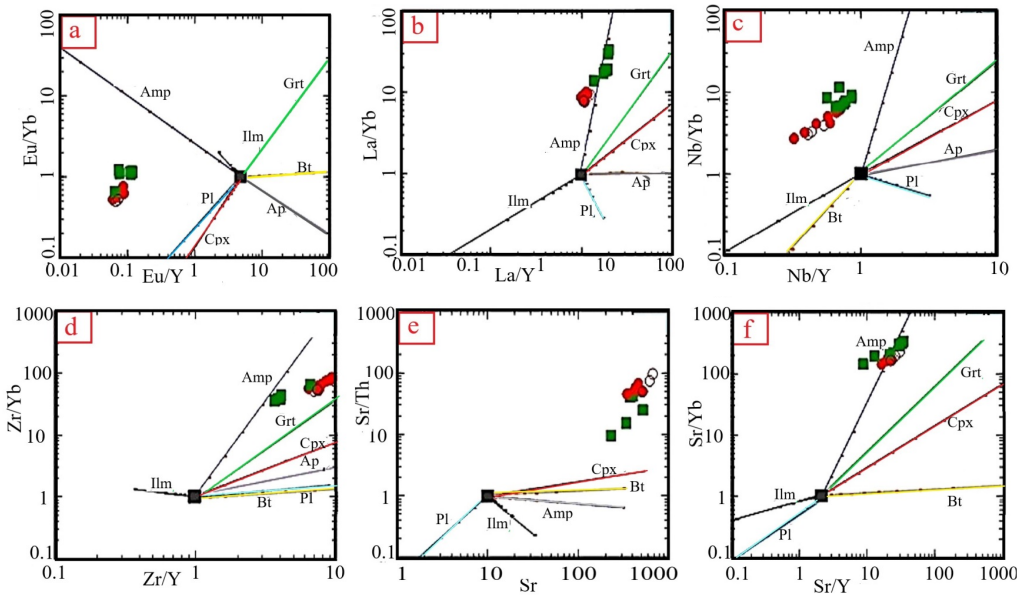

Figure 5. Geochemical-mineralogical diagrams for a) and b) REEs c) and d) HFSEs, e) and f) LILEs (Keskin, 2002); Abbreviations for minerals were extracted from Whitney and Evans (2010). Pl = Plagioclase; Cpx = Clinopyroxene; Bt = Biotite; Amp = Amphibole; Ap = Apatite; Ilm = Ilmenite; Grt = Garnet.

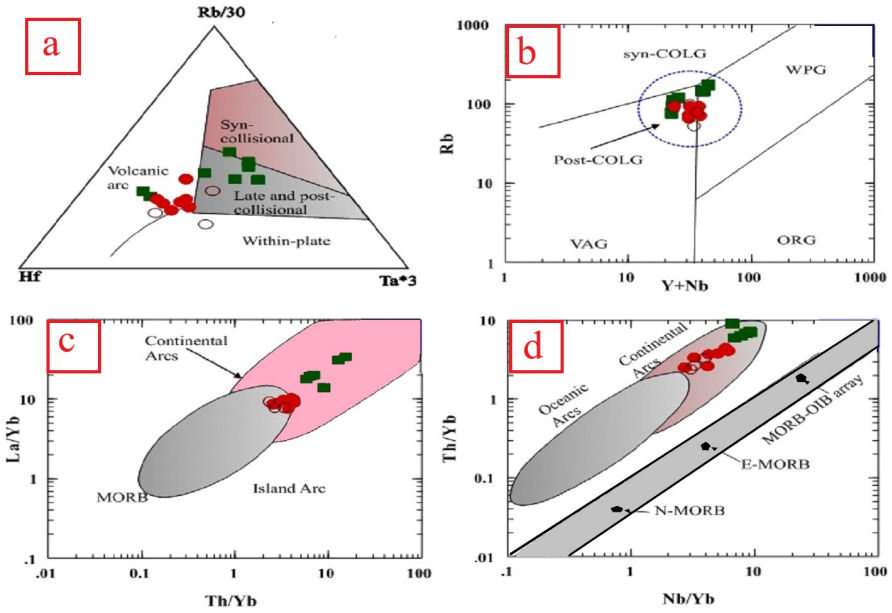

Figure 6. Characteristic diagrams of tectonic environments: a) Rb/30-Hf-Ta × 3 (Harris et al., 1986), b) Rb vs. Y + Nb (Pearce et al., 1984), c) La/Yb vs. Th/Yb, and d) Th/Yb vs. Nb/Yb (Pearce et al., 1984); the studied samples show the post-collision tectonic environment related to continental arcs.

1984)Figs. 6e and 6d), all rock samples are in the continental arc range. Based on tectonic environment separation diagrams, these samples are located in volcanic arc fields. Thus, it is likely that they have formed in a volcanic arc related to the oceanic crust subduction.

SiO_2 content of Yuzbashi Chay volcanic rocks is in the range of 51 to 67 wt.%. In comparison, the SiO_2 content of magma from molten material is less than 57 wt.% (Baker et al., 1995), suggesting that these rocks do not make the primary magma produced from partial melting. Similarly, Mg# values for the primary arc melts are usually greater than 70 (Schmidt and Jagoutz, 2017) While this ratio is $29-54$ in the studied rocks. This result means that these volcanic rocks are formed from mantle-derived magma after differential crystallization in the magma chamber (Xu et al., 2019). The concentrations of LILEs and LREEs and negative anomalies of Nb, Ta, and Ti suggest that the origin of these rocks is not an asthenospheric mantle like OIB or MORB (Hofmann, 1997). In addition, asthenosphere-derived basalts have a high Nb to La ratio (> 1) and a low Th to Nb ratio (< 1) (Saunders et al., 1992). These ratios are inconsistent with those of the studied samples (i.e., Nb/La = 0.28 to 0.67 and Th/Nb = 0.64 to 1.49). Therefore, it is unlikely that a completely mantle source from the asthenosphere is responsible for the formation of these volcanic rocks. In fact, negative anomalies of Nb-Ti, positive anomalies of Pb a (Fig. 4), high La/Ba ratios (1.50 to 3.51), and low La/Ba ratios (0.03 to 0.05) show the typical features of a subducted modified lithosphere mantle (Fig. 7a, (Saunders et al., 1992)). Fluid-bearing melts have a much higher HFSE transfer potential than aqueous liquid phases. In comparison, LILEs can be transported more efficiently in these media instead of being melted by liquids (Hermann et al., 2006; Chen et al., 2018). Therefore, the relative

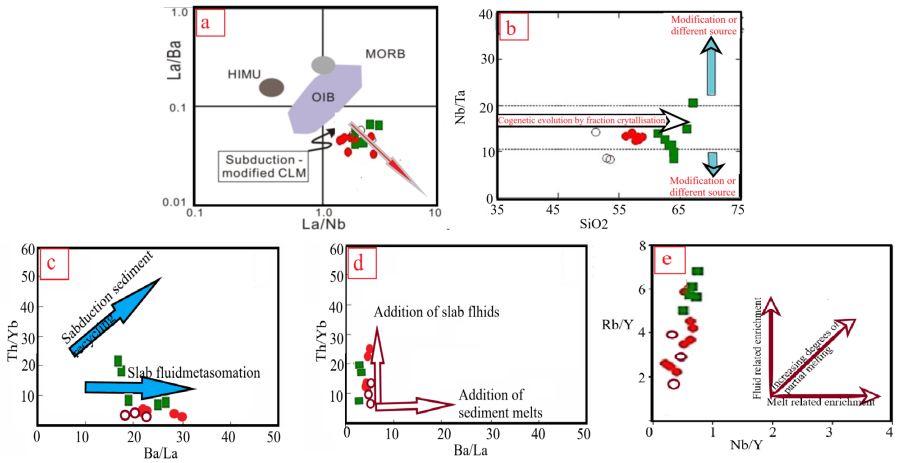

Figure 7. a) La/Ba vs. La/Nb (Saunders et al., 1992), b) Nb/Ta vs. SiO_2 (Marilyn & Gontier, 2020), indicating a common lithospheric origin for the studied samples; c) Th/Yb vs. Ba/La, d) Sr/La vs. La/Yb (Saunders et al., 1992); e) Rb/Y vs. Nb/Y (Bhat et al., 2019), indicating the role of slab fluids in the petrogenesis of these rocks.

contribution of two metasomatic factors in the formation of the studied volcanic rocks can be sought using the ratio of trace elements that have a certain fluid mobility (Chen et al., 2018). To identify the role of slab-related fluids and enrichment process, we used trace element ratio variation diagrams of Sr/L vs. La/Yb, Th/Yb vs. Ba/La (Saunders et al., 1992), Nb/Y vs. Rb/Y (Bhat et al., 2019) (Fig. 7b, 7c, and 7d). All samples show evidence for plate metasomatism and represent a mantle origin affected by metasomatism. As shown in Figs. 7, the samples examined have a wide range of Ba/La ratios (18.68 to 36.50) but uniformed Th/Yb ratios (2.31 – 12.47), indicating the important role of fluids from slabs in the petrogenesis of these rocks.

6. Subduction-modified CLM: Subduction-modified crust contaminated with the lithospheric mantle

According to (**Shervais2019**), the average crystallization of olivine, plagioclase and clinopyroxene does not affect the ratio of some HFS elements (e.g., Zr/Nb, La/Sm, La/Yb, Ce/Yb). Hence, their variations are used to obtain differences in the melting degree and even infer the relative depth of melting (Wendt et al., 1999; Condie, 2005; Pearce, 2008; Gounti´e-Dedzo et al., 2019; Asaah et al., 2020). Diagrams of some of these ratios for the examples in this study are provided in Fig. 8.

According to the diagram proposed by (Chen et al., 2013), all samples are placed on the melting curve of peridotite garnet with a melting degree of 5 to 20% (Fig. 8a). Fig. 8b shows the variations of Sm against the Sm/Y (Zhao and Zhou, 2007) for the studied volcanic rocks. As can be noticed from this figure, the studied samples in terms of abundance of Sm and Yb have a similar composition to the melt derived from the enriched mantle. Overall, we suggest that the magma of these rocks is most likely produced by partial melting of mantle wedge enriched by liquids derived from metasomatized slabs. Studying the Sm/Yb versus Sm indicates that the studied volcanic rocks have a low-to-medium melting degree (20 – 5) from a Garnet-Spinel lherzolite mantle (Fig. 8b).

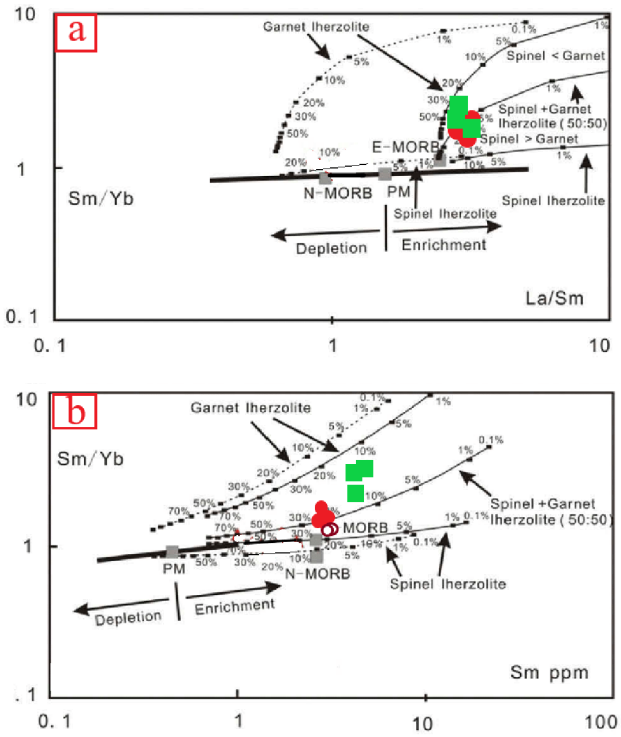

Figure 8. a) the La/Yb vs. Sm/Yb diagram (Chen et al., 2013) and b) Sm/Yb vs. Sm diagram (Zhao and Zhou, 2007).

7. Determination of plagioclase and clinopyroxene minerals based on the chemical composition

A. Plagioclase

On a triangular Or-Ab-An chart from Deer et al., 1991 (Fig. 9), plagioclases from the igneous rocks of the study area fall in the Labradorite and Bitonite zone. The chemical composition of plagioclase phenocrysts varies from An89.94Ab8.56Or1.48 to An95.93 Ab3.67Or0.36 in basaltic andesite, from $An_{99.95}Ab_{0}Or_{0.47}$ to $An_{70.23}Ab_{24.80}Or_{4.95}$ in basaltic andesite to basalt, and $An_{1.26}Ab_{24.52}Or_{4.21}$ in basalts.

B. Pyroxene

The classification diagram proposed by Morimoto et al., 1988, was used to determine the exact type of pyroxenes. Pyroxenes have a composition range of diopside to augite. The approximate chemical composition of clinopyroxene phenocrysts is $En_{39.93}$ Fs_{0} $Wo_{60.06}$ in basalts and En_{0} $Fs_{3.93}$ $Wo_{59.5}$ to $En_{35.20}$ $Fs_{6.30}$ $Wo_{96.90}$ in andesitic basalts.

8. Techno-magmatic environment

The Neotethys ocean has formed and expanded due to the creation of the Upper Carboniferous-Early Permian rift in the south of the Cimmerian plate (Bront et al., 2003; Glonka et al., 2004). This collision did not happen simultaneously, but it happened obliquely and gradually so that first Alborz and then Lut block collided on the Turan continental shelf (Glunka et al., 2004). After the Eocene, the subduction slope has changed. This slope change has led to the upwelling of mantle materials (Verdel et al., 2011).

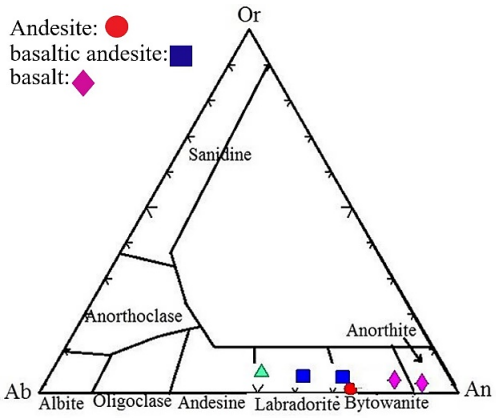

Figure 9. The triangular Or-Ab-An chart from Deer et al., 1991; in this figure, circle, square, and diamond denotes andesite, basaltic andesite, and basalt, respectively.

The migration of these enriched magmas and their mixing with crust magmas cause the creation of dual-composition rocks. Dual-state volcanic assemblages usually occur in post-collision extension tectonic settings, within fractures, or back-arc fractures (Zhang et al., 2008; Chen et al., 2013; Su et al., 2018; Zhang et al., 2017; Chen et al., 2018). Fig. 10 presents a schematic tectonomagmatic model for the magmatism origin in the study area (inspired by (Verdel et al., 2011; Moghadam et al., 2018)). Late Eocene-Miocene magmatic activity in central Alborz might be due to slab rollback and probably an extension regime (Keshtkar and Ghorbani, 2016). Therefore, according to this model, these rocks have formed due to the rollback of the subducted plate during subduction and mantle magma upwelling and melting of young mafic continental crust beneath this belt due to lithospheric extension during the Late Eocene (Figs. 5-8). The expansion of the asthenosphere provides the heat motor required to melt the crust. As a result, the asthenosphere is decompressed and then upwelled to provide the heat needed to melt the lower crust and form the studied rocks. After melting the lower crust and forming these rocks, this heating source may be affected by magmatic transformation processes such as crystallization and digestion of crustal rocks and contamination with crustal materials, and thus become alkaline in nature. Slab rollback (in the back of the subduction plate) in the asthenosphere mantle leads to the overflow of the young asthenospheric mantle. The upwelling asthenosphere mass probably settles in the shallow asthenosphere in the lower lithosphere (80 km >) and creates a small-scale geochemical heterogeneity. Accordingly, magma forms a basin at the base of the crust that can transfer heat and mass to the lower crust, allowing more crust to be produced and assimilated. Hence, calc-alkaline pyroxene and magnetite are formed without plagioclase to produce these volcanic rocks.

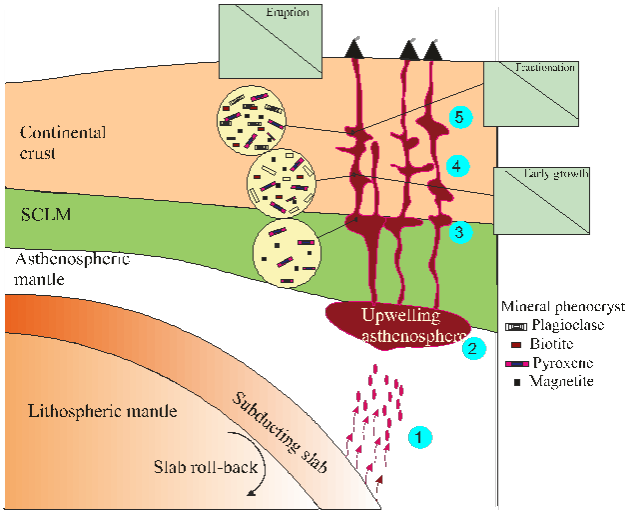

Figure 10. Schematic of tectonic evolution and subduction of the oceanic lithosphere of Neotethys below the Iranian plate in Western during the Eocene: 1) Source enrichment with water and melted sediments, 2) partial melting of subduction plate of peridotite mantle, 3) Pool creation at the base of the crust allows segregation of calc-alkaline pyroxene and magnetite to produce high alumina basalts, 4) Crust assimilation and differential crystallization of calc-alkaline plagioclase, amphibole, biotite, and zircon, 5) Differential crystallization and crustal contamination.

Overall, it is concluded that the high Al content, as a result of extensive differential crystallization with delay in plagioclase, was probably due to high water content instead of high-pressure crystallization. Thus, the magma forming the studied rocks originated from the hydrated asthenospheric mantle wedge, located on the subduction plate of the oceanic lithosphere. Meanwhile, crustal assimilation differentiates plagioclase, calc-alkaline pyroxene, magnetite, amphibole, and biotite. Ultimately, initial melting leads to forming low magnesium and high alumina basalts. As shown in Fig. 10, in the aqueous magma pool at the base of the crust, crustal assimilation and differentiation of calc-alkaline pyroxene and magnetite occur without plagioclase and zircon. Accordingly, magma upwelling through the crust leads to the crystallization of plagioclase and finally zircon. In general, the partial melting of the metasomatized continental lithosphere mantle (SCLM) leads to forming of mafic volcanic rocks. Meanwhile, partial crystallization of mafic magma causes intermediate and felsic volcanic rocks.

9. Conclusion

Field surveys and mineralogical, petrographical, geochemical, and petrological studies of volcanic rocks, including lava and tuff, show that volcanic rocks were acidic in the Early Eocene and intermediate and basic in the Late Eocene. Various types of rocks were identified, including basalt, basaltic andesite, andesite, trachyandesite, trachyte, rhyodacite, and rhyolite tuffs. Geochemical studies showed that the specimens are located in the calc-alkaline-alkaline range, and all rocks are in the high potassium-shoshonitic range, confirming their lithosphere mantle and role of differential crystallization in the evolution of Yuzbashchai volcanic rocks. These volcanic rocks at high depths ($70-80$ km) have formed in an enriched mantle source and a rollback setting.

Authors contributions
Authors have contributed equally in preparing and writing the manuscript.

Availability of data and materials
The data that support the findings of this study are available from the corresponding author, upon reasonable request.

Conflict of interests
The authors declare that they have no known competing financial interests or personal relationships that could have appeared to influence the work reported in this paper.

References

Aghazadeh M., Castro A., Badrzadeh Z., Vogt K. (2011) Post-collisional polycyclic plutonism from the Zagros hinterland: the Shaivar Dagh plutonic complex, Alborz belt, Iran. *Geological Magazine* 148 (5-6): 980–1008. DOI: https://doi.org/10.1017/S0016756811000380.

Annells R.N., Arthurton R.S., Bazely R.A., Davies R.G. (1975) Explanatory text of the Qazvin and Rasht quadrangles map1:250000, G.S.I. Rep. No. E3, E4, 94.

Arjmandzadeh R., Sharifi Teshnizi E., Rastegarnia A., Golian M., Jabbari P., Shamsi H., Tavasoli S. (2020) GIS-Based Landslide Susceptibility Mapping in Qazvin Province of Iran. *Iranian Journal of Science and Technology, Transactions of Civil Engineering* 44 (Suppl 1): 619–647. DOI: https://doi.org/10.1007/s40996-019-00326-3.

Asaah A.N.E., Yokoyama T., Aka F.T., Iwamori H., Kuritani T., Usui T., Gounti´eDedzo M., et al. (2020) Major/trace elements and Sr-Nd-Pb isotope systematics of lavas from lakes Barombi Mbo and Barombi Koto in the Kumba graben, Cameroon volcanic line: Constraints on petrogenesis. *African Earth Sci.* 161 DOI: https://doi.org/10.1016/j.jafrearsci.2019.103675.

Asiabanha A. (2001) Geology and petrogenesis of volcanic facies at the Uzbashichai area, west of Qazvin, PhD thesis, University of Tarbiyat Modares. 231.

Asiabanha A., Ghassemi H., Meshkin M. (1989) Paleogene continental arc type volcanism in north Qazvin, north Iran: facies analysis andbasalts as petrogenetic indicator. *Chemical Geology* 77 (3): 165–182. DOI: https://doi.org/10.1127/0077-7757/2009/0144.

Baker M.B., Hirschmann M.M., Ghiorsot M.S., Stolper E.M. (1995) Compositions of nearsolidus peridotite melts from experiments and thermodynamic calculations. *Nature* 375:308–311. DOI: https://doi.org/10.1038/375308a0.

Bhat I.M., Ahmad T., Rao D.S. (2019) The tectonic evolution of the Dras arc complex along the Indus Suture Zone, western Himalaya: Implications for the Neo-Tethys Ocean geodynamics. *Geodyn* 124:52–66. DOI: https://doi.org/10.1016/j.jog.2019.01.015.

Chen L., Zheng Y.F., Zhao Z.F. (2018) A common crustal component in the sources of bimodal magmatism: geochemical evidence from Mesozoic volcanics in the Middle-Lower Yangtze Valley, South China. *Geological Society of America Bulletin* 130:1959–1980.

Chen X., Shu L., Santosh M., Zhao X. (2013) Island arc-type bimodal magmatism in the eastern Tianshan Belt, Northwest China: Geochemistry, zircon U–Pb geochronology and implications for the Paleozoic crustal evolution in Central Asia. *Lithos* 168-169:48–66. DOI: https://doi.org/10.1016/j.lithos.2012.10.006.

Conceicao R.V., Green D.H. (2004) Derivation of potassic (shoshonitic) magmas by decompression melting of phlogopite+pargasite lherzolite. *Journal of Geology* 72:209–229. DOI: https://doi.org/10.1016/j.lithos.2003.09.003.

Condie K.C. (2005) High Field strength element ratios in Archean basalts: a window to evolving sources of mantle plumes? *Lithos* 79:491–504. DOI: https://doi.org/10.1016/j.lithos.2004.09.014.

Dilek Y., Imamverdiyev N., Altunkaynak Ş. (2010) Geochemistry and tectonics of Cenozoic volcanism in the Lesser Caucasus (Azerbaijan) and the peri-Arabian region: collision induced mantle dynamics and its magmatic fingerprint. *International Geology Review* 52:536–578. DOI: https://doi.org/10.1080/00206810903360422.

Elliott T. (2003) Tracers of the slab. in Eiler, J., eds., Inside the subduction factory: Washington". American Geophysical Union. *Geophysical Monograph* 138:23–45. DOI: https://doi.org/10.1029/138GM03.

Floyd P.A., Winchester J.A. (1977) Magma type and tectonic setting discrimination using immobile elements. *Earth Planet* 27:211–218.

Frost B.R., Barnes C.G., Collins W.J., Arculus R.J., Ellis D.J., Frost C.D. (2001) A geochemical classification for granitic rocks. *Journal of Petrology* 42:2033–2048. DOI: https://doi.org/10.1093/petrology/42.11.2033.

Ghasempour M.R., Mehdipour Ghazi J., Biabangard H., Dabiri R. (2014) Petrogenetic Evolution of Plio-Quaternary Mafic Lavas in Nehbandan (East Iran). *Iranian Journal of Earth Sciences* 6 (1): 133–141.

Gill R. (2010) Igneous Rocks and Processes. *Wiley-Blackwell* (Malaysia), 440.

Gounti´e-Dedzo M., Asaah A.N.E., Martial Fozing E., Chako-Tchamab´e B., Tefogoum Zangmo G., Dagwai N., Tchokona Seuwui D., Kamgang P., Aka F.T., Ohba T. (2019) Petrology and geochemistry of lavas from Gawar, Minawao and Zamay volcanoes of the northern segment of the Cameroon volcanic line (Central Africa): constraints on mantle source and geochemical evolution. *Geochemistry* 80 (4): 31–41. DOI: https://doi.org/10.1016/j.chemer.2020.125663.

Harris N.B.W., Pearce J.A., Tindle A.G. (1986) Geochemical characteristics of collision-zone magmatism. *Geological Society Special Publications* 19:67–81.

Hermann J., Spandler C., Hack A., Korsakov A.V. (2006) Aqueous fluids and hydrous melts in high pressure and ultra-highpressure rocks: implications for element transfer in subduction zones *Lithos* 92:399–417.

Hofmann A.W. (1997) Mantle geochemistry: the message from oceanic volcanism. *Nature* 9385:219–229. DOI: https://doi.org/10.1016/0043-1354(80)90143-8.

Jahangiri A. (2007) Post-collisional Miocene adakitic volcanism in NW Iran: geochemical and geodynamic implications. *Journal of Asian Earth Sciences* 30 (3-4): 433–447.

Jiang Y.H., Jiang S.Y., Ling H.F., Zhou X.R., Rui X.J., Yang W.Z. (2002) Petrology and geochemistry of shoshonitic plutons from the western Kunlun orogenic belt, Xinjiang, northwestern China: implications for granitoid genesis. *Lithos* 63:165–187. DOI: https://doi.org/10.1016/S0024-4937(02)00140-8.

Kamber B.S., Ewart A., Collerson K.D., Bruce M.C., Donald G.D. (2002) Fluid-mobile trace element constraints on the role slab melting and implication for Archean crustal growth models. *Contribution to Mineralogy and Petrology* 144:38–56. DOI: https://doi.org/10.1007/s00410-002-0374-5.

Kelemen P.B., Hanghoj K., Greene A.R. (2003) One view of the geochemistry of subduction-related magmatic arcs, with an emphasis on primitive andesite and lower crust. *Treatise on Geochemistry* 3:593–659. DOI: https://doi.org/10.1016/B0-08-043751-6/03035-8.

Keshtkar I., Ghorbani M. (2016) Petrology and geochemistry of intrusive masses of Karaj-Taleghan axis. (PhD thesis in Petrology, Shahid Beheshti University, Tehran.), 324.

Keskin M. (2002) FC-Modeler: a Microsoft® Excel© spreadsheet program for modeling Rayleigh fractionation vectors in closed magmatic systems *Computers & Geosciences* 28:919–928. DOI: https://doi.org/10.1016/S0098-3004(02)00010-9.

Leuthold J., Müntener O., Baumgartner L.P., Putlitz B., Chiaradia M. (2013) A detailed geochemical study of a shallow arc-related laccolith, the Torres del Paine mafic complex (Patagonia). *Journal of Petrology* 54:273–303. DOI: https://doi.org/10.1093/petrology/egs069.

Mobashergarmi M. (2013) Petrological, petrographical and geochemical studies of basaltic rocks in south Germi (Ardabil province). (MSc thesis, University of Tabriz, Tabriz, Iran, (in Persian).)

Moghadam H.S., Griffin W.L., Li X.H., Santos J.F., Karsli O., Stern R.J., Ghorbani G., Gain S., Murphy R., OReilly S.Y. (2018) Extension and Mantle Upwelling Triggered Eocene Potassic Magmatism in NW Iran. *Journal of Petrology* 59 (7): 1417–1465. DOI: https://doi.org/10.1093/petrology/egy067.

Moghadam H.S., Stern R.J., Griffin W., Khedr M., Kirchenbaur M., Ottley C., Gain S. (n.d.)

Mollai H., Dabiri R., Torshizian H., Pe-Piper G., Wang W.E.I. (2021) Upper Neoproterozoic garnet-bearing granites in the Zeber-Kuh region from east central Iran micro plate: Implications for the magmatic evolution in the northern margin of Gondwanaland. *Geologica Carpathica* 72 (6): 461–481. DOI: https://doi.org/10.31577/GeolCarp.72.6.2.

Nabavi M.H. (1976) An Introduction to Geology of Iran, Geological Survey of Iran. 109P.

Nazari M., Arian M.A., Solgi A., Zareisahamieh R., Yazdi A. (2023) Geochemistry and tectonomagmatic environment of Eocene volcanic rocks in the Southeastern region of Abhar, NW Iran. *Iranian Journal of Earth Sciences* 15 (4): 228–247. DOI: https://doi.org/10.30495/ijes.2023.1956689.1746.

Ousta S.h., Ashja-Ardalan A., Yazdi A., Dabiri R., Arian M.A. (2024) Petrogenesis and tectonic implications of Miocene dikes in the southeast of Bam (SE Iran): Constraints on the development of active continental margin. *Geopersia* 14 (1): 89–111. DOI: https://doi.org/10.22059/geope.2023.364334.648729.

Pearce J.A. (2008) Geochemical fngerprinting of oceanic basalts with applications to ophiolite classifcation and the search for Archean oceanic crust. *Lithos* 100:14–48. DOI: https://doi.org/10.1016/j.lithos.2007.06.016.

Pearce J.A., Harris N., Tindle A.G. (1984) Trace element discrimination diagrams for the tectonic interpretation of granitic rocks. *Journal of Petrology* 24 (5): 956–983.

Pearce J.A., Peate D. (1995) Tectonic implications of the composition of volcanic arc magmas. *Annual Review of Earth and Planetary Sciences* 23:251–286.

Perfit M., Gust D., Bence A.E., Arculus R., Taylor S. (1980) Chemical characteristics of island-arc basalts: implications formantle sources. *Chemical Geology* 30:227–256. DOI: https://doi.org/10.1016/0009-2541(80)90107-2.

Sarikhani R., Ghasemi Dehnavi A., Zarei Sahamiyeh R., Moradpour A. (2017) Investigation of magmatic rocks and environmental effects of alteration zones in the region of Yuzbashi Chay (west of Qazvin). *New Findings of Applied Geology* 11 (21): 34–50. DOI: https://doi.org/10.22084/nfag.2017.1922.

Saunders A.D., Storey M., Kent R.W., Norry M.J. (1992) Consequences of plume–lithosphere interactions: Storey, B.C., Alabaster, T., and Pankhurst, R.J., eds., Magmatism and the cause of Continental breakup. *Geological Society of Special Publication* 68:41–60.

Schmidt M.W., Jagoutz O. (2017) The global systematics of primitive arc melts. *Geochem. Geophys. Geosyst* 18:2817–2854. DOI: https://doi.org/10.1002/2016GC006699.

Shafaii Moghadam M.H., Shahbazi Shiran S.H. (2010) Geochemistry and petrogenesis of volcanic rocks from the northern part of the Lahrud region(Ardabil): an example of shoshonitic occurrence in northwestern Iran. *Journal of Petrology* 1 (4): 16–31.

Stocklin J. (1968) Structural history and tectonics of Iran, A review. *AAPG Bulletin* 52 (7): 1229–1258.

Su W.B., Cai K.D., Sun M., Wan B., Wang X.S., Bao Z.H., Xiao W.J. (2018) Carboniferous volcanic rocks associated with back-arc extension in the western Chinese Tianshan, NW China: insight from temporal-spatial character, petrogenesis and tectonic significance. *Lithos* 310-311:241–254. DOI: https://doi.org/10.1007/s00531-021-02111-y.

Sun S.S., McDonough W.F. (1989) Chemical and isotopic systematics of oceanic basalts: implications for mantle composition and processes, In: Saunders, A. D. and Norry M. J. (eds), Magmatism in ocean basins. *Geological Society* (London) 42:313–345.

Swain G., Barovich K., Hand M., Ferris G., Schwarz M. (2008) Petrogenesis of the St Peter Suite, southern Australia: Arc magmatism and Proterozoic crustal growth of the South Australian Craton. *Precambrian Research* 166:283–296. DOI: https://doi.org/10.1016/j.precamres.2007.07.028.

Tatsumi Y., Hamilton D.L., Nesbitt R.W. (1986) Chemical characteristics of fluid plase released from a subducted lithosphere and origin of arc magmas: evidence from high pressure experiments and natural rocks. *Journal of Volcanology* 29:293–310. DOI: https://doi.org/10.1016/0377-0273(86)90049-1.

Teshnizi E.S., Golian M., Sadeghi S., Rastegarnia A. (2022) Application of analytical hierarchy process (AHP) in landslide susceptibility mapping for Qazvin province, N Iran. *Computers in Earth and Environmental Sciences,* 55–95. DOI: https://doi.org/10.1016/B978-0-323-89861-4.00041-5.

Verdel C., Wernicke B.P., Hassanzadeh J., Guest B. (2011) A Paleogene extensional arc flare-up in Iran. *Tectonics* 30:TC3008. DOI: https://doi.org/10.1029/2010TC002809.

Wendt J.I., Regelous M., Niu H. Y, ekinian R., Collerson K.D. (1999) Geochemistry of lavas from the garrett transform fault: insights into mantle heterogeneity beneath the eastern pacific. *Earth Planet Sci* 173:271–284. DOI: https://doi.org/10.1016/S0012-821X(99)00236-8.

Whitney D.L., Evans B.W. (2010) Abbreviations for names of rock-forming minerals *American Mineralogist* 95:158–187. DOI: https://doi.org/10.2138/am.2010.3371.

Wyllie P.J., Skine T. (1982) The formation of mantle phlogopite in subduction zone hybridization. *Contribution to Mineralogy and Petrology* 79:375–380.

Xu W., Zhu D.C., Wang Q., Weinberg R.F., Wang R., Li S.M., Zhang L.L., Zhao Z.D. (2019) Constructing the Early Mesozoic Gangdese crust in southern Tibet by hornblende dominated magmatic differentiation. *Journal of Petrology* 60 (3): 515–552. DOI: https://doi.org/10.1093/petrology/egz005.

Zanchi A., Berra F., Mattei M., Ghassemi M.R., Sabouri J. (2006) Inversion tectonics in Central Iran. *Journal of Structural Geology* 28:2023–2037. DOI: https://doi.org/10.1016/j.jsg.2006.06.020.

Zarei Sahamieh R. (1992) Petrography, Petrology, and Geochemistry of North Abhar Volcanic Rocks and the Relationship between Volcanism in the Region and Mineralization. *M.Sc. Thesis, Faculty of Science, Tarbiat Moallem University*

Zhang X.H., Zhang H.F., Tang Y.J., Wilde S.A., Hu Z.C. (2008) Geochemistry of Permian bimodal volcanic rocks from central Inner Mongolia, North China: implication for tectonic setting and Phanerozoic continental growth in Central Asian Orogenic Belt. *Chemical Geology* 249:262–281. DOI: https://doi.org/10.1016/j.chemgeo.2008.01.005.

Zhang Y.Y., Yuan C., Long X.P., Sun M., Zhang Y., Du L., Wang X.Y. (2017) Carboniferous bimodal volcanic rocks in the Eastern Tianshan, NW China: evidence for arc rifting. *Gondwana Research* 43:92–106. DOI: https://doi.org/10.1016/j.gsf.2019.06.003.

Zhao J.H., Zhou M.F. (2007) Geochemistry of Neoproterozoic mafic intrusions in the Panzhihua district (Sichuan province, SW China). implications for subduction-related metasomatism in the upper mantle. *Precambrian Research* 152:27–47. DOI: https://doi.org/10.1016/j.precamres.2006.09.002.

Zheng Y.F. (2019) Subduction zone geochemistry. *Geosci* 4:1223–1254. DOI: https://doi.org/10.1016/j.gsf.2019.02.003.